NIH Public Access
Author Manuscript

Int J Cancer. Author manuscript; available in PMC 2014 August 13.

NF-κB inhibition significantly upregulates the norepinephrine transporter system, causes apoptosis in pheochromocytoma cell lines and prevents metastasis in an animal model

Karel Pacak[1], **Marta Sirova**[2,*], **Alessio Giubellino**[1,*], **Lubomira Lencesova**[2], **Lucia Csaderova**[3], **Sona Hudecova**[2], and **Olga Krizanova**[2]

[1]Program in Reproductive and Adult Endocrinology, Eunice Kennedy Shriver National Institute of Child Health and Human Development, National Institutes of Health, Bethesda, Maryland 20892, USA

[2]Institute of Molecular Physiology and Genetics, Slovak Academy of Sciences, Bratislava, Slovak Republic

[3]Molecular Medicine Center, Slovak Academy of Sciences, Bratislava, Slovak Republic

Abstract

Pheochromocytomas (PHEOs) and paragangliomas (PGLs) are specific types of neuroendocrine tumors that originate in the adrenal medulla or sympathetic/parasympathetic paraganglia, respectively. Although these tumors are intensively studied, a very effective treatment for metastatic PHEO or PGL has not yet been established. Preclinical evaluations of novel therapies for these tumors are very much required. Therefore, in the present study we tested the effect of triptolide (TTL), a potent nuclear factor-kappaB (NF-κB) inhibitor, on the cell membrane norepinephrine transporter system (NET), considered to be the gatekeeper for the radiotherapeutic agent ^{131}I-metaiodobenzylguanidine (^{131}I-MIBG). We measured changes in the mRNA and protein levels of NET and correlated them with proapoptotic factors and metastasis inhibition. The study was carried out on three different stable pheochromocytoma cell lines.

We found that blocking NF-κB with TTL or capsaicin (KPSC) increased both NET mRNA and protein levels. Involvement of NF-κB in the upregulation of NET was verified by mRNA silencing of this site and also by using NF-κB antipeptide. Moreover, MIBG transport was increased in TTL-treated cells and *in vivo* treatment with TTL significantly reduced metastatic burden in a metastatic animal model of pheochromocytoma.

The present study for the first time shows mechanistically how NF-κB inhibitors can be successfully used in the treatment of metastatic PHEO/PGL by a significant upregulation of NET to increase the efficacy of ^{131}I-MIBG and by the induction of apoptosis.

Correspondence should be addressed to: Olga Krizanova, PhD, DSc, Associate Professor of Pharmacology, Director, Institute of Molecular Physiology and Genetics, Slovak Academy of Sciences, Vlarska 5, 833 34 Bratislava, Slovak Republic, Phone: +421 2 54775266, Fax: +421 2 54773666, olga.krizanova@savba.sk. Karel Pacak, MD, PhD, DSc, Senior Investigator, Chief, Section on Medical Neuroendocrinology, Professor of Medicine, Eunice Kennedy Shriver NICHD, NIH, Building 10, CRC, Room 1E-3140, 10 Center Drive MSC-1109, Bethesda, Maryland 20892-1109 USA, Phone: (301) 402-4594, FAX: (301) 402-4712, karel@mail.nih.gov.
*These authors contributed equally to the work

DISCLOSURE STATEMENT: The authors have nothing to disclose.

Keywords

NF-κB inhibition; pheochromocytoma; apoptosis; norepinephrine transporter

Introduction

Pheochromocytomas (PHEOs) and paragangliomas (PGLs) are neuroendocrine tumors that originate from chromaffin cells of the adrenal medulla or paraganglia. These tumors are mainly sporadic, but if associated with a succinate dehydrogenase subunit B gene mutation, they are almost invariably metastatic and fatal [1, 2]. However, the treatment of metastatic PHEO/PGL is very challenging; currently there is almost no cure and traditional chemotherapeutic treatments have been rather suboptimal or ineffective [3, 4, 5]. Furthermore, studying outcomes of new forms of treatment has been difficult because the low prevalence of malignant disease makes it difficult to assemble adequately sized study cohorts [6].

Triptolide (TTL), a diterpene triepoxide, is a purified compound from *Tripterygium* that has been identified as one of the major components responsible for the immunosuppressive and antiinflammatory effects of this herb [7]. Nevertheless, the antiproliferative and proapoptotic activity of TTL has been shown in many different types of cancer cells *in vitro* and *in vivo* [8, 9]. Shamon et al. [8] found that TTL can block the growth of human mammary tumor cells in nude mice. Tengchaisri et al. [10] reported that TTL inhibits the growth of cholangiocarcinoma cells in hamsters. TTL may also be a promising candidate to test for antitumor activity against prostate cancer [11]. The antiinflammatory, antiproliferative and proapoptotic properties of TTL have been proposed to be associated with the inhibition of nuclear factor-kappaB (NF-κB) [12].

For metastatic PHEO and/or PGL, ^{131}I-metaiodobenzylguanidine (^{131}I-MIBG) therapy is currently the most efficient nonsurgical therapeutic modality for inoperable, disseminated disease [13, 14, 15]. ^{131}I-MIBG results in the accumulation of ^{131}I in tumor cells and their destruction by high-energy β irradiation. ^{131}I-MIBG enters the PHEO/PGL cell using the cell membrane catecholamine transporter, the so-called norepinephrine transporter (NET) [16]. The frequently seen suboptimal response to ^{131}I-MIBG is likely related to reduced expression of NET and to the number of catecholamine storage granules in metastatic PHEO or PGL. This suboptimal response is often seen in patients with succinate dehydrogenase subunit B (SDHB)-related PHEOs/PGLs, which are the most aggressive and metastatic tumors as compared to other PHEOs/PGLs (Pacak; unpublished observations). Thus, several attempts have been done to increase the expression of NET, e.g. recently through the use of histone deacetylase inhibitors to allow ^{131}I-MIBG to enter a PHEO/PGL cell and destroy it by β radiation [17]. Since Padbury et al. [18] already published that the rat NET promoter contains two NF-κB sites, the aim of the present study was (a) to increase the expression of NET by a novel approach using the inhibition of NF-κB as a pretreatment option for patients undergoing ^{131}I-MIBG therapy, and (b) to introduce NF-κB inhibitors as a new potential treatment option for metastatic PHEO/PGL. TTL was used as an NF-κB inhibitor in three stable PHEO cell lines: the rat PC12 cell line and the mouse PHEO (MPC) and mouse tumor

tissue (MTT) cell lines. TTL efficacy was evaluated *in vivo* using a mouse model of metastatic PHEO and magnetic resonance imaging (MRI).

Material and Methods

Cell cultivation and treatment

PC12 cells (German Collection of Microorganisms and Cell Cultures, Braunschweig, Germany) derived from a rat PHEO were cultured in Minimal Essential Medium of Dulbecco (DMEM; Biochrom AG, Berlin, Germany) with high glucose (4.5 g/l) supplemented with 15% fetal calf serum and penicillin and streptomycin antibiotics. MPC and MTT cells derived from mouse PHEOs [19] were cultured in RPMI 1640 Medium (RPMI; Biochrom AG, Berlin, Germany) with high glucose (4.5 g/l) supplemented with 20% fetal calf serum and penicillin and streptomycin antibiotics. All cells were cultured in a water-saturated atmosphere at 37°C and 5% CO_2.

Treatment of cells with TTL and KPSC

MPC and MTT cells were treated with 10, 100 and 500 nM TTL (Tocris Bioscience) for 24 hrs and 200 μM (E)-capsaicin (KPSC; Merck, Germany) for 24 hrs. Afterwards cells were used for RNA isolation, Western blot analysis and detection of apoptosis with Annexin-V-Fluos (Roche Diagnostics, Germany).

Silencing of the NF-κB gene

For this experiment, 5×10^3 MPC and/or MTT cells were seeded to each well. Prior to siRNA treatment, cells were washed 3 times with RPMI without serum. For silencing, On Target Plus Smart Pool Mouse Rela (Thermo Scientific, USA) silencer was used. Transfection was done with the X-tremeGENE siRNA transfection reagent (Roche Diagnostics, Germany), according to the manufacturer protocol. Cells with siRNA were incubated 4 hours at 37°C in serum-free medium. After 4 hours, serum was added to the cells and they were incubated for an additional 24, 48 or 72 hours. Since silencing was most effective after 48 hours, all experiments were performed at this time period.

Treatment with antisense NF-κB protein

Prior to treatment, cells were washed gently with 1 ml of RPMI without fetal calf serum. Afterwards, cells were treated with NF-κB SN50 cell-permeable inhibitor peptide (Calbiochem, Germany) in serum-free RPMI. Transfection was done with ProteoJuice™ Protein Transfection Reagent (Novagen), according to the manufacturer protocol. The length of time that the cells were exposed to the transfection mixture was optimized to 4 hours. Afterwards, cells were scraped and used for further experiments.

RNA isolation and relative quantification of mRNA levels by RT-PCR

For isolation of RNA, cells were scraped and centrifuged. The total RNA was isolated by the TRI Reagent method (MRC Ltd., USA). Briefly, cells were homogenized in TRI Reagent and after 5 minutes the homogenate was extracted by chloroform and RNAs in the aqueous phase were precipitated by isopropanol. The RNA pellet was washed in 75% ethanol and

stored in 96% ethanol at −70°C. The purity and integrity of the isolated RNAs were checked on the GeneQuant Pro spectrophotometer (Amersham Biosciences). Reverse transcription was performed using 1.5 μg of total RNAs and Ready-To-Go You-Prime First-Strand Beads (GE Healthcare-Life Sciences, UK) with pd(N6) primer. PCR specific for NET, caspase 3 and cyclophilin A (CYCLO) was performed as described in Lencesova et al. [20]. Products were analyzed in a 2% agarose gel and signals were evaluated by PCBAS 2.0 software.

Western blot analysis

Cells were scraped and resuspended in 10 mM Tris-HCl, pH 7.5, 1 mM phenylmethyl sulfonylfluoride (PMSF, Serva, Germany), protease inhibitor cocktail tablets (Complete EDTA-free, Roche Diagnostics, Germany) and subjected to centrifugation for 10 min at 10,000 × g at 4°C. The pellet was resuspended in Tris buffer containing 50 μM CHAPS (3-[(3-Cholamidopropyl)dimethyl-ammonio] 1-propanesulfonate, Sigma, USA), and then incubated for 10 min at 4°C. The lysate was centrifuged for 10 min at 10,000 × g at 4°C. The protein concentration of the supernatants was determined by the method of Lowry et al. [21]. 40 μg of protein extract from each sample was separated by electrophoresis on 10% SDS polyacrylamide gels and proteins were transferred to the Hybond-P membrane using semidry blotting (Owl, Inc., USA). Membranes were blocked in 5% non-fat dry milk in Tris-Buffered Saline with Tween 20 (TBS-T) overnight at 4°C and then incubated for 1 hr with rabbit anti-rat NET polyclonal primary antibody (Millipore, USA). Following washing, membranes were incubated with secondary antibody to rabbit IgG conjugated to horseradish peroxidase for 1 hr at room temperature. An enhanced chemiluminiscence detection system (ECL Plus, Amersham Biosciences) was used to detect bound antibody. The optical density of individual bands was quantified using PCBAS 2.0 software.

Immunofluorescence

For immunofluorescence, cells were fixed with ice-cold methanol. In these experiments, rabbit anti-rat NET affinity purified polyclonal antibody (Millipore Corporation, CA, USA) directed against a 22 amino acid peptide sequence mapping to the first extracellular domain of rat NET was used. This sequence is 100% conserved in mouse NET protein. Cells grown on glass coverslips were fixed in ice-cold methanol at −20°C for 5 min. Non-specific binding was blocked by incubation with PBS containing 3% BSA for 60 min at 37°C. Cells were then incubated with primary antibody diluted 1:500 in PBS with 1% BSA (PBS-BSA) for 1 h at 37°C, washed three times with PBS-BSA for 10 min, incubated with CF Fluor® 488 goat anti-rabbit IgG (Biotinium, Hayward, USA) diluted 1:1000 in PBS-BSA for 1 h at 37°C and washed as previously. Finally, cells were mounted onto slides in mounting medium with Citifluor (Agar Scientific Ltd., Essex, UK), analyzed by a Leica DM450B fluorescent microscope with Leica DFC 480 and Leica IM 500 software and also by a Zeiss LSM510 laser scanning confocal microscopy system mounted on a Zeiss Axiovert 200M inverted microscope. Images were taken with a Plan Apochromat 63x/1.4 oil objective. Images were scanned at scan speed 7 (260 Hz line frequency), 512×512 pixels, 12 Bit data depth with an average mode 4x line at optical zoom 2, 4 or 6. The Z-stack interval was 0.3 μm and images were scanned at 512×512 pixels, 12 Bit data depth without averaging at optical zoom 6.

Detection of apoptosis with Annexin-V-FITC

MPC and MTT cells were washed with PBS and pelleted at $200 \times g$ for 5 min. The cell pellet from each well was resuspended in 100 ml of Annexin-V-FITC labeling solution and incubated at room temperature in the dark for 20 min. Labeling solution contained incubation buffer with 10 mM HEPES/NaOH pH 7.4, 140 mM NaCl and 5 mM CaCl2, 2 ml of Annexin-V-FITC (Roche Diagnostics, Germany) and 0.02 mg propidium iodide. After the incubation, cells were washed with 5 ml of PBS, pelleted at $200 \times g$ for 5 min, resuspended in 300 ml of PBS and measured on an EPICS ALTRA flow cytometer (Beckman Coulter, Fullerton, USA).

MIBG measurements

MTT cells were seeded in 6 well plates, 1 [0–9] $\times$ [0–9] 10^4 cells in each well. After 24 hours, 6 wells were treated with 30 μM MIBG (final concentration), 6 wells were treated with 100 nM TTL (final concentration) (as negative controls) and 6 wells were treated with 100 nM TTL with 30 μM MIBG. After an additional 24 hours, the medium was removed and cells were washed 3 times with RPMI medium. After the last wash, the medium was removed and cells were scraped into sterile water, where they were lysed. Debris was removed by centrifugation and the amount of MIBG was detected at 254 nm [22, 23].

Animal experiments

MTT cells were grown in tissue culture tissue until 80% confluency, then incubated in 0.05% trypsin EDTA (Gibco) for 3 minutes at 37°C, gently detached and counted. Cells were then resuspended in PBS and 5×10^5 cells were injected into the tail vein of female athymic nude mice (Taconic, Germantown, MD). The experimental group consisted of 10-week-old mice (n=6) housed in a pathogen-free facility. All animal studies were conducted in accordance with the principles and procedures outlined in the NIH Guide for the Care and Use of Animals and approved by the NIH ACUC Committee. The animals were treated daily starting from the fourth day post-cell injection with 0.15 mg/kg/day (intraperitoneal (i.p.) injection). Control animals were treated daily in parallel with vehicle only. Four weeks later the mice were imaged as described below (MRI imaging) and then euthanized using CO_2 inhalation and cervical dislocation. Livers from the mice were dissected and preserved in 10% formalin.

MRI imaging

For MRI, anesthesia was induced in a chamber with 5% isoflurane in an 80%/20% medical air/oxygen mixture. The mouse was then transferred to a cradle with a built-in mask and anesthesia was maintained at 30–45 breaths per minute with 1–2% isoflurane. All scans were performed using a 7 Tesla Bruker Biospec system (Bruker-Biospin, Billerica, MA) and a 35 mm linear bird cage coil. Each data set consisted of an initial locator scan, followed by a T_2-weighted scan and a proton density weighted scan. To reduce motion artifacts, the acquisition was gated so that acquisition occurred between breaths (Small Animal Instruments, Inc. Stony Brook, NY). T_2-weighted images consisted of twelve 1 mm slices over a 6×3 cm FOV acquired using a RARE (Rapid Acquisition Relaxation Enhanced) sequence. The image matrix was 256×256 and 4 echoes were acquired per excitation.

Images were analyzed using OsiriX Imaging Software (http://www.osirix-viewer.com), and quantitative measurements of the number of lesions were conducted. Results on the number of lesions in the livers are presented as mean ± standard error of the mean (S.E.M.). Statistical significance was assessed by an unpaired t-test, with P value < 0.01 set as significant.

Histopathology

In order to confirm the presence of PHEO tumor cells, we removed the livers from the mice and preserved them in 10% formalin immediately after *in vivo* imaging. Tissues were paraffin embedded, sectioned and stained with hematoxylin and eosin, and analyzed by microscopy using a Leica microscope.

Statistical analysis

Each value represents the average of 5–15 wells from at least 3 independent cultivations of PC12, MPC, or MTT cells. Results are presented as mean ± S.E.M. Statistical differences among groups were determined by one-way analysis of variance (ANOVA). Statistical significance of $p < 0.05$ was considered to be significant. For multiple comparisons, an adjusted t-test with p values corrected by the Bonferroni method was used (Instat, GraphPad Software, USA).

Results

TTL affects NET cellular expression in PHEO cells and affects apoptosis

In order to estimate the effect of NF-κB inhibition on NET expression, the PHEO cell lines MPC and MTT were treated for 24 hours with a range of effective concentrations starting at 10 nM, to a maximal concentration of 500 nM of the NF-κB inhibitor TTL. In MPC cells, NET mRNA increased significantly after treatment with a concentration as low as 10 nM TTL, while in MTT cells, which represent a more aggressive cell line, 100 nM TTL was needed to observe a significant increase of NET mRNA levels (Figure 1A).

To verify that the increased mRNA expression correlated with a corresponding increase in translation, we performed a similar treatment and analyzed the cells for NET protein expression. Treatment with 100 nM TTL significantly increased NET protein in both MPC and MTT cells, as determined by Western blot analysis (Figure 1B).

Considering the role of NF-κB in the control of apoptosis, we wanted to determine whether inhibition with TTL affects this important survival pathway. For this reason we determined mRNA expression levels of the protease caspase 3, which has been established to have an essential role in the execution-phase of cell apoptosis. The caspase 3 mRNA level showed a significant increase after TTL treatment in all tested concentrations, reflecting an increase in apoptosis in MPC (Figure 1C) and MTT cells (Figure 1C) after treatment.

Moreover, a significant increase in NET immunofluorescence occurred in both MPC and MTT cells after 100 and/or 500 nM TTL treatment (Figure 2A). Specificity of NET signal was verified by negative control (NC), where primary NET antibody was omitted. When cells were treated with 500 nM TTL, debris from dead MTT cells was visible (Figure 2A,

white arrows). The immunofluorescent signal was quantified (Figure 2B) and confirmed increased NET after the TTL treatment.

Similarly, increase in the NET mRNA (Figure 3A), NET protein (Figure 3B) and NET immunofluorescent signal (Figure 3C) was determined in PC12 cells, suggesting the specific effect of TTL on all PHEO cell lines.

KPSC induces an increase in NET expression and affects apoptosis

KPSC, another NF-κB inhibitor, also significantly increased NET mRNA in both MPC (left) and MTT (right) cells (Figure 4, **upper part**). Moreover, upregulation of the caspase 3 mRNA was observed (Figure 4, **bottom part**). Combined treatment of TTL and KPSC did not reveal an additional increase, thus suggesting that the mechanism of the NET mRNA increase might be the same. Similarly, an increase in NET mRNA was demonstrated after NF-κB siRNA silencing (sil) in PC12 and MPC cell lines (Figure 5B). In order to show that TTL acts through the NF-κB site, NET mRNA was measured in cells treated with a combination of both TTL and sil. In this combination, no additional increase in NET mRNA was observed compared to TTL and/or sil (Figure 5B). Thus, based on these results we propose that TTL might act through the inhibition of the NF-κB site. The effect of the NF-κB blocking was verified by the NF-κB antisense peptide (AP) in MPC and MTT (Figure 5A) cells. In accordance with TTL treatment, treatment with AP also significantly increased NET mRNA in both cell types. Induction of apoptosis and/or apoptosis/necrosis was significantly increased in both MPC and MTT cells (Figure 5C, D). Apoptosis/necrosis was more pronounced in MPC cells (Figure 5C), while in the more aggressive MTT cells only apoptosis was significantly increased after AP treatment (Figure 7D). The combined effect of TTL and AP was not significantly different from AP, thus suggesting a similar mechanism of action.

TTL inhibits tumor growth in a model of metastatic pheochromocytoma

The positive results obtained *in vitro* prompted us to investigate the effect of TTL in an animal model of PHEO. For this reason we used an animal model of metastatic PHEO we have recently described [19]. This model takes advantage of the aggressive nature of the mouse PHEO cell line MTT. MTT cells (5×10^5) were injected into the tail vein of 10-week-old nude mice. Subsequently, two groups were generated: one group of animals was assigned to the treatment arm and injected daily with 0.15 mg/kg/day, i.p., of TTL; the second group was injected with a control vehicle following the same schedule. Respiratory-triggered T2-weighted MRI images were collected four weeks later and representative images are presented in Figure 6 (**panel A**). As shown in this Figure, metastatic MTT tumor cells vastly invaded the liver parenchyma of the untreated mice (**upper images**), leaving only small portions of the liver without lesions. In contrast, in animals treated with TTL only few or no metastases were detectable by MRI, demonstrating a very potent effect of this compound *in vivo* in nearly eradicating metastatic growth in the liver, which represents the major metastatic site in this animal model. The number of liver lesions was then analyzed using software analysis of the MRI acquired and the differences are represented in Figure 6 (**panel B**). The amount of MIBG transported to the cells was higher in TTL-treated cells compared to controls (Figure 6, **panel C).**

After MRI scanning, mice were euthanized and their livers were dissected. Figure 7 (**panel A**) represents the gross anatomy of treated versus control animal livers; the number of macroscopic lesions visible on the hepatic surface of the control mice clearly contrasts with the absence of metastatic lesions on the surface of the liver of treated mice, which conserve a smooth and clear appearance. This observation is in agreement with the radiologic analysis illustrated in Figure 7 and further emphasizes the striking effect of the compound in reducing metastatic burden. Histopathology analysis of sectioned livers confirmed the reduced number of metastatic lesions in the hepatic parenchyma (Figure 7, **panel B and C**).

Discussion

In the present study, we demonstrated for the first time that NF-κB inhibition significantly upregulates NET and induces apoptosis in various PHEO cell lines. Furthermore, we have shown that NF-κB inhibition using TTL resulted in a significant reduction of liver metastases in an animal model of metastatic PHEO. These results clearly support the introduction of a novel metastatic cancer therapeutic option using NF-κB inhibitors, of which there are several currently in clinical trials, in patients with metastatic PHEO or PGL.

NET expression is prominent in chromaffin cells of the adrenal gland and extra-adrenal paraganglia, as well as in the neoplastic derivatives of chromaffin cells, PHEOs and PGLs [24]. In addition to its role as a target for psychostimulants, such as cocaine, and several antidepressants, NET also plays a key role in PHEO/PGL-specific imaging and treatment modalities using agents such as ^{131}I-MIBG [14, 15, 25, 26] and ^{18}F-fluorodopamine (^{18}F-FDA) [27, 28]. For this reason, NET represents a crucial area of current interest for those who study PHEO and PGL as well as other tumors of neural crest lineage, including neuroblastoma. A greater understanding of the regulation and expression profile of NET will undoubtedly enhance the use of agents that rely on NET activity for diagnostic and treatment modalities, mainly ^{131}I-MIBG, not only for PHEO or PGL but also for other tumors such as neuroblastoma and some carcinoids.

In the present study we have found that TTL, a diterpenoid triepoxide (Mr 360) derived from the herb *Tripterygium wilfordii*, significantly increased gene expression and also protein levels of NET. Increase in NET mRNA was concentration dependent and corresponded with the expression of the proapoptotic protein caspase 3. Several reports have indicated that TTL inhibits the proliferation of cancer cells *in vitro* and reduces the growth of some tumors *in vivo* [29, 8, 10]. Although TTL is known to activate a number of pathways within the cell, its specific upstream target remains unclear. Indeed, it is possible that TTL may target multiple molecules critical to cell survival. These molecules may, in turn, activate the various pathways that lead to suppression of the cell cycle and induction of apoptosis, which inhibit the growth of primary and metastatic tumors [30].

TTL is known to act as an inhibitor of NF-κB. Originally discovered as a transcription factor regulating immunoglobulin gene expression, NF-κB has now been assigned numerous physiological and pathological functions. Activation of NF-κB through inhibitory phosphorylation of IκB by the IKK complex leads to the nuclear translocation of NF-κB, where it stimulates the transcription of target genes that are involved in immune responses,

inflammation and cell survival [31]. It has been demonstrated that NF-κB controls the expression of various anti-apoptotic proteins including XIAP, IAP and gadd45α which inhibit caspase-dependent apoptosis and also encode target genes that inhibit c-Jun N-terminal kinase (JNK) activation [32, 33, 34]. Thus, consistent with the function of NF-κB in regulating cell growth and survival, deregulated NF-κB activation is linked to oncogenesis. It is now a well-known phenomenon that the NF-κB signaling pathway is constitutively activated in various cancer cells. Recently it was shown that inhibition of NF-κB acts as a tumor suppressor in NK/T or B cell lymphoma [35, 36]. However, how NF-κB regulates cancer development remains incompletely understood and, in some cases, even largely controversial. In order to verify our proposal that an inhibition of the NF-κB is responsible for the increase in NET expression, we treated cells with another NF-κB inhibitor, KPSC, and also with NF-κB mRNA silencing and NF-κB antipeptide. In all these cases we observed NET upregulation. Moreover, treatment with a combination of TTL with any of these compounds did not show an additional increase compared to TTL treatment alone, which would point to an effect through the same active site, NF-κB. All these results support the importance of NF-κB inhibition in NET upregulation.

Previously, inhibition of NF-κB by different compounds was suggested to induce apoptosis in PC12 cells [37, 38]. In the present study we observed a rapid increase of apoptosis and apoptosis/necrosis after TTL treatment or treatment with NF-κB antisense peptide. Interestingly, in MPC cells 24 hour treatment resulted in pronounced apoptosis/necrosis, especially after NF-κB antisense treatment, while in MTT cells, only a degree of apoptosis was increased. Since MTT cells are known to be more aggressive than MPC cells [19], the effect of NF-κB inhibition might be weaker or delayed. Apoptosis induction due to suppression of NF-κB has already been described [39, 40]. Pratheeshkumar and Kuttan [40] have shown that oleanolic acid also induces apoptosis through suppression of the NF-κB-induced Bcl-2 mediated apoptotic pathway.

Our *in vivo* animal model of metastatic PHEO further demonstrated the significant effect of NF-κB inhibition on metastatic PHEO liver lesions. Specifically, in animals treated with TTL, only few or no PHEO liver metastases were detectable by MRI compared to those animals without TTL treatment. These results for the first time identify NF-κB as a biologically relevant therapeutic target for these tumors, including their metastatic lesions. Indeed, a recently performed clinical trial entitled "Efficacy of NF–κB Inhibition for Reducing Symptoms During Maintenance Therapy in Multiple Myeloma Patients" (NCT01269203) stressed the importance of NF-κB inhibition in cancer diagnosis and/or treatment of cancer.

In summary, we have shown for the first time that TTL increases gene expression and protein levels of NET through inhibition of NF-κB. Moreover, this inhibition results in the pronounced increase of apoptosis and significantly decreases the size of metastases. From these results we propose the use of NF-κB inhibitors in patients with metastatic PHEO or PGL, either to increase the efficacy of ^{131}I-MIBG treatment or as an agent to affect tumor growth by inducing apoptosis.

Acknowledgments

References

1. Brouwers FM, Kant JA, Adams KT, Linehan WM, Tao JJ, Eisenhofer G, et al. High frequency of SDHB germline mutations in patients with malignant catecholamine-producing paragangliomas: Implications for genetic testing. J Clin Endocrinol Metab. 2006; 91:4505–9. [PubMed: 16912137]

2. Amar L, Bertherat J, Baudin E, Ajzenberg C, Bressac-de Paillerets B, Chabre O, et al. Genetic testing in pheochromocytoma or functional paraganglioma. J Clin Oncol. 2005; 23:8812–8. [PubMed: 16314641]

3. Scholz T, Eisenhofer G, Pacak K, Dralle H, Lehnert H. Current treatment of malignant pheochromocytoma. J Clin Endocrinol Metab. 2007; 92:1217–25. [PubMed: 17284633]

4. Huang H, Abraham J, Hung E, Averbuch S, Merino M, Steinberg SM, et al. Treatment of malignant pheochromocytoma/paraganglioma with cyclophosphamide, vincristine, and dacarbazine: recommendation from a 22-year follow-up of 18 patients. Cancer. 2008; 113:2020–8. [PubMed: 18780317]

5. Druce MR, Kaltsas GA, Fraenkel M, Gross DJ, Grossman AB. Novel and evolving therapies in the treatment of malignant phaeochromocytoma: experience with the mTOR inhibitor everolimus (RAD001). Horm Metab Res. 2009; 41:697–702. [PubMed: 19424940]

6. Pacak K, Eisenhofer G, Ahlman H, Bornstein SR, Gimenez-Raqueplo AP, Grossman AB, et al. Pheochromocytoma: Recommendations for clinical practice from the First International Symposium. October 2005. Nat Clin Pract Endocrinol Metab. 2007; 3:92–102. [PubMed: 17237836]

7. Kupchan SM, Court WA, Dailey RG Jr, Gilmore CJ, Bryan RF. Triptolide and tripdiolide, novel antileukemic diterpenoid triepoxides from Tripterygium wilfordii. J Am Chem Soc. 1972; 94:7194–5. [PubMed: 5072337]

8. Shamon LA, Pezzuto JM, Graves JM, Mehta RR, Wangcharoentrakul S, Sangsuwan R, et al. Evaluation of the mutagenic, cytotoxic, and antitumor potential of triptolide, a highly oxygenated diterpene isolated from Tripterygium wilfordii. Cancer Lett. 1997; 112:113–7. [PubMed: 9029176]

9. Liu Q. Triptolide and its expanding multiple pharmacological functions. Int Immunopharmacol. 2011; 11:377–83. [PubMed: 21255694]

10. Tengchaisri T, Chawengkirttikul R, Rachaphaew N, Reutrakul V, Sangsuwan R, Sirisinha S. Antitumor activity of triptolide against cholangiocarcinoma growth in vitro and in hamsters. Cancer Lett. 1998; 133:169–75. [PubMed: 10072166]

11. Kiviharju TM, Lecane PS, Sellers RG, Peehl DM. Antiproliferative and proapoptotic activities of triptolide (PG490), a natural product entering clinical trials, on primary cultures of human prostatic epithelial cells. Clin Cancer Res. 2002; 8:2666–74. [PubMed: 12171899]

12. Lee KY, Chang W, Qiu D, Kao PN, Rosen GD. PG490 (triptolide) cooperates with tumor necrosis factor-alpha to induce apoptosis in tumor cells. J Biol Chem. 1999; 274:13451–5. [PubMed: 10224110]

13. Grunwald F, Ezziddin S. 131I-metaiodobenzylguanidine therapy of neuroblastoma and other neuroendocrine tumors. Semin Nucl Med. 2010; 40:153–163. [PubMed: 20113683]

14. Gonias S, Goldsby R, Matthay KK, Hawkins R, Price D, Huberty J, et al. Phase II study of high-dose [131]metaiodobenzylguanidine therapy for patients with metastatic pheochromocytoma and paraganglioma. J Clin Oncol. 2009; 27:4162–8. [PubMed: 19636009]

15. Rose B, Matthay KK, Price D, Huberty J, Klencke B, Norton JA, et al. High-dose 131l-metaiodobenzylguanidine therapy for 12 patients with malignant pheochromocytoma. Cancer. 2003; 98:239–48. [PubMed: 12872341]

16. Bayer M, Kuci Z, Schomig E, Grundemann D, Dittmann H, Handgretinger R, et al. Uptake of mIBG and catecholamines in noradrenaline- and organic cation transporter-expressing cells:

potential use of corticosterone for a preferred uptake in neuroblastoma- and pheochromocytoma cells. Nucl Med Biol. 2009; 36:287–94. [PubMed: 19324274]

17. Martiniova L, Perera SM, Brouers FM, Alesci S, Abu-Asab M, Marvelle AF, et al. Increased uptake of [123I]meta-iodobenzylguanidine, [18F]fluorodopamine, and [3H]norepinephrine in mouse pheochromocytoma cells and tumors after treatment with the histone deacetylase inhibitors. Endocr Relat Cancer. 2011; 18:143–57. [PubMed: 21098082]

18. Padbury JF, McGonnigal B, Tseng YT, Nguyen TT, Stabila JP. Cloning and sequence analysis of the rat norepinephrine transporter promoter. Brain Res Mol Brain Res. 2000; 83:128–32. [PubMed: 11072103]

19. Martiniova L, Lai EW, Elkahloun AG, Abu-Asab M, Wickremasinghe A, Solis DC, et al. Characterization of an animal model of aggressive metastatic pheochromocytoma linked to a specific gene signature. Clin Exp Metastasis. 2009; 26:239–50. [PubMed: 19169894]

20. Lencesova L, Sirova M, Csaderova L, Laukova M, Sulova Z, Kvetnansky R, et al. Changes and role of adrenoceptors in PC12 cells after phenylephrine administration and apoptosis induction. Neurochem Int. 2010; 57:884–92. [PubMed: 20888879]

21. Lowry OH, Rosebrough NJ, Farr AL, Randall RJ. Protein measurement with the Folin phenol reagent. J Biol Chem. 1951; 193:265–75. [PubMed: 14907713]

22. Smets LA, Loesberg C, Janssen M, Van Rooij H. Intracellular inhibition of mono (ADP-ribosylation) by meta-iodobenzylguanidine: specifity, intracellular concentration and effect on glucocorticoid-mediated cell lysis. Biochimica et Biophysica Acta. 1990; 1054:49–55. [PubMed: 2143421]

23. Wafelman AR, Konings MC, Rosing H, Hoefnagel CA, Taal BG, Maes RA, et al. High-performance liquid chromatographic determination of metaiodobenzylguanidine in whole blood and plasma of cancer patients. J Pharm Biomed Anal. 1994; 12:1173–9. [PubMed: 7803569]

24. Cleary S, Phillips JK. The norepinephrine transporter and pheochromocytoma. Ann NY Acad Sci. 2006; 1073:263–9. [PubMed: 17102094]

25. Sisson JC, Shulkin BL. Nuclear medicine imaging of pheochromocytoma and neuroblastoma. Q J Nucl Med. 1999; 43:217–23. [PubMed: 10568137]

26. Loh KC, Fitzgerald PA, Matthay KK, Yeo PP, Price DC. The treatment of malignant pheochromocytoma with iodine-131 metaiodobenzylguanidine (131I-MIBG): a comprehensive review of 116 reported patients. J Endocrinol Invest. 1997; 20:648–58. [PubMed: 9492103]

27. Pacak K, Eisenhofer G, Carrasquillo JA, Chen CC, Li ST, Goldstein DS. 6-[18F]fluorodopamine positron emission tomographic (PET) scanning for diagnostic localization of pheochromocytoma. Hypertension. 2011; 38:6–8. [PubMed: 11463751]

28. Ilias I, Yu J, Carrasquillo JA, Chen CC, Eisenhofer G, Whatley M, et al. Superiority of 6-[18F]fluorodopamine positron emission tomography versus [131I]-metaiodobenzylguanidine scintigraphy in the localization of metastatic pheochromocytoma. J Clin Endocrinol Metab. 2003; 88:4083–4087. [PubMed: 12970267]

29. Chang WT, Kang JJ, Lee KY, Wei K, Anderson E, Gotmare S, et al. Triptolide and chemotherapy cooperate in tumor cell apoptosis. A role for the p53 pathway. J Biol Chem. 2001; 276:2221–7. [PubMed: 11053449]

30. Yang S, Chen J, Guo Z, Xu XM, Wang L, Pei XF, et al. Triptolide inhibits the growth and metastasis of solid tumors. Mol Cancer Ther. 2003; 2:65–72. [PubMed: 12533674]

31. Karin M, Cao Y, Greten FR, Li ZW. NF-kappaB in cancer: from innocent bystander to major culprit. Nat Rev Cancer. 2002; 2:301–10. [PubMed: 12001991]

32. De Smaele E, Zazzeroni F, Papa S, Nguyen DU, Jin R, Jones J, et al. Induction of gadd45beta by NF-kappaB downregulates pro-apoptotic JNK signalling. Nature. 2001; 414:308–13. [PubMed: 11713530]

33. Tang G, Minemoto Y, Dibling B, Purcell NH, Li Z, Karin M, et al. Inhibition of JNK activation through NF-kappaB target genes. Nature. 2001; 6861:313–7. [PubMed: 11713531]

34. Tang F, Tang G, Xiang J, Dai Q, Rosner MR, Lin A. The absence of NF-kappaB-mediated inhibition of c-Jun N-terminal kinase activation contributes to tumor necrosis factor alpha-induced apoptosis. Mol Cell Biol. 2002; 22:8571–9. [PubMed: 12446776]

35. Paik JH, Jang JY, Jeon YK, Kim WY, Kim TM, Heo DS, et al. MicroRNA-146a downregulates NF{kappa}B activity via targeting TRAF6, and functions as a tumor suppressor having strong prognostic implications in NK/T cell lymphoma. Clin Cancer Res. 2011 in press.

36. Gaurnier-Hausser A, Patel R, Baldwin AS, May MJ, Mason N. NEMO binding domain peptide inhibits constitutive NF-{kappa}B activity and reduces tumor burden in a canine model of relapsed, refractory Diffuse Large B-Cell Lymphoma. Clin Cancer Res. 2011 in press.

37. Kiss K, Kiss J, Rudolf E, Cervinka M, Szeberenyi J. Sodium salicylate inhibits NF-kappaB and induces apoptosis in PC12 cells. J Biochem Biophys Methods. 2004; 29:229–40. [PubMed: 15560939]

38. Lee SY, Lee JW, Lee H, Yoo HS, Yun YP, Oh KW, et al. Inhibitory effect of green tea extract on beta-amyloid-induced PC12 cell death by inhibition of the activation of NF-kappaB and ERK/p38 MAP kinase pathway through antioxidant mechanisms. Brain Res Mol Brain Res. 2005; 140:45–54. [PubMed: 16153742]

39. Martinon F, Holler N, Richard C, Tschopp J. Activation of a pro-apoptotic amplification loop through inhibition of NF-kappaB-dependent survival signals by caspase-mediated inactivation of RIP. FEBS Lett. 2000; 468:134–6. [PubMed: 10692573]

40. Pratheeshkumar P, Kuttan G. Vernolide-A, a sesquiterpene lactone from Vernonia cinerea, induces apoptosis in B16F-10 melanoma cells by modulating p 53 and caspase-3 gene expressions and regulating NF-kappaB-mediated bcl-2 activation. Drug Chem Toxicol. 2011; 34:261–70. [PubMed: 21649480]
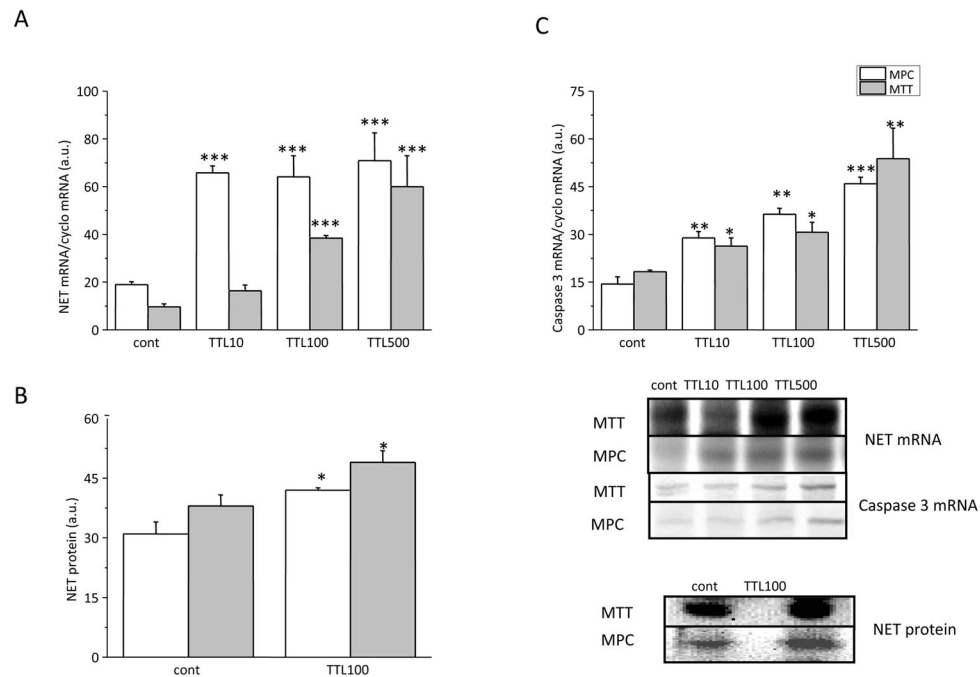
Figure 1.
Effect of TTL on the gene expression of NET (**A**), NET protein (**B**) and caspase 3 (**C**) in MPC and MTT cells. **A)** Both cell lines were treated with three different concentrations of TTL – 10, 100 and 500 nM for 24 hours. While in MTT cells increase of NET mRNA occurs in a concentration dependent manner, in MPC cells we observed a steep increase starting at a lower dose (10 nM) of TTL. **B)** Increase in NET protein levels was observed in both types of cells after the treatment with 100 nM TTL. **C)** After TTL treatment a significant increase in caspase 3 mRNA occurred in both cell lines, although this increase was more pronounced in MPC cells. Results are displayed as mean ± S.E.M. and represent an average of at least five parallels from two independent cultivations. Statistical significance compared to control represents * - p>0.05 and *** - p>0.001.
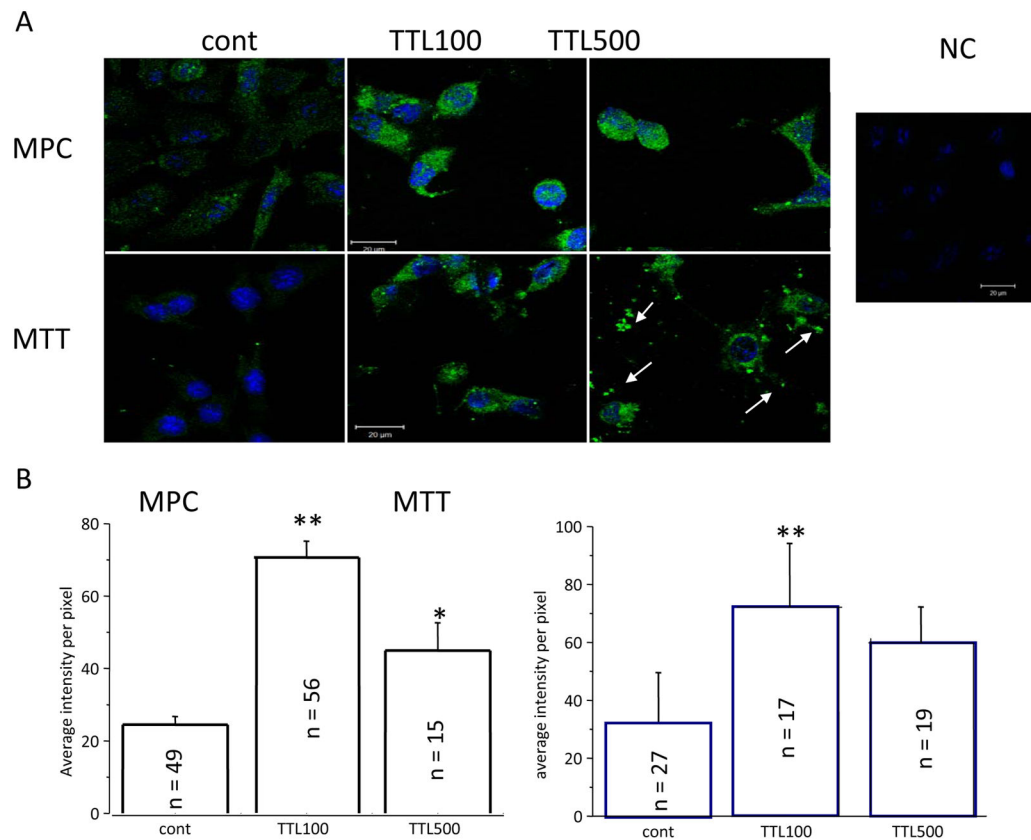
Figure 2.
Immunofluorescence with NET antibody after 100 and 500 nM TTL treatment. **A)** After TTL treatment, green immunofluorescent signal for NET was much stronger compared to untreated cells (cont) in both the MPC and MTT lines. Nuclei are stained with DAPI. After treatment with 500 nM TTL, change of shape is visible and debris, probably from dead cells, arises (white arrows). The negative control (NC) proved the specificity of NET signal. **B)** Quantification of the NET fluorescent signal also revealed a significant increase after TTL treatment compared to untreated control cells. Number of cells (n) included in the evaluation is shown inside each column.
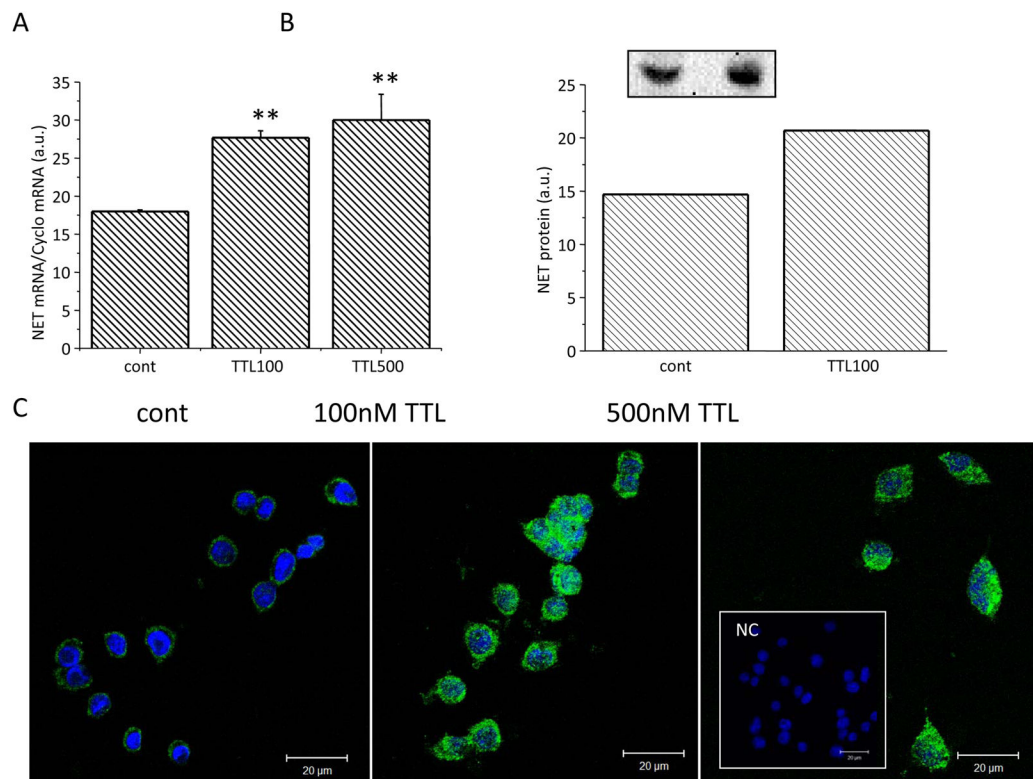
Figure 3.
Effect of TTL on the gene expression of NET (**A**), NET protein levels (**B**) and immunofluorescence (**C**) in PC12 cells. PC12 cell lines were treated with two different concentrations of TTL, 100 and 500 nM, for 24 hours. NET mRNA and protein were increased after the TTL treatment in PC12 cells. After TTL treatment, the green immunofluorescent signal for NET was much stronger compared to untreated PC12 cells (cont). Nuclei are stained with DAPI. The negative control (**NC**, inset) proved the specificity of the NET signal. Results are displayed as mean ± S.E.M. and represent an average of at least five parallels from two independent cultivations. Statistical significance compared to control represents * - $p > 0.05$, ** - $p > 0.01$ and *** - $p > 0.001$.
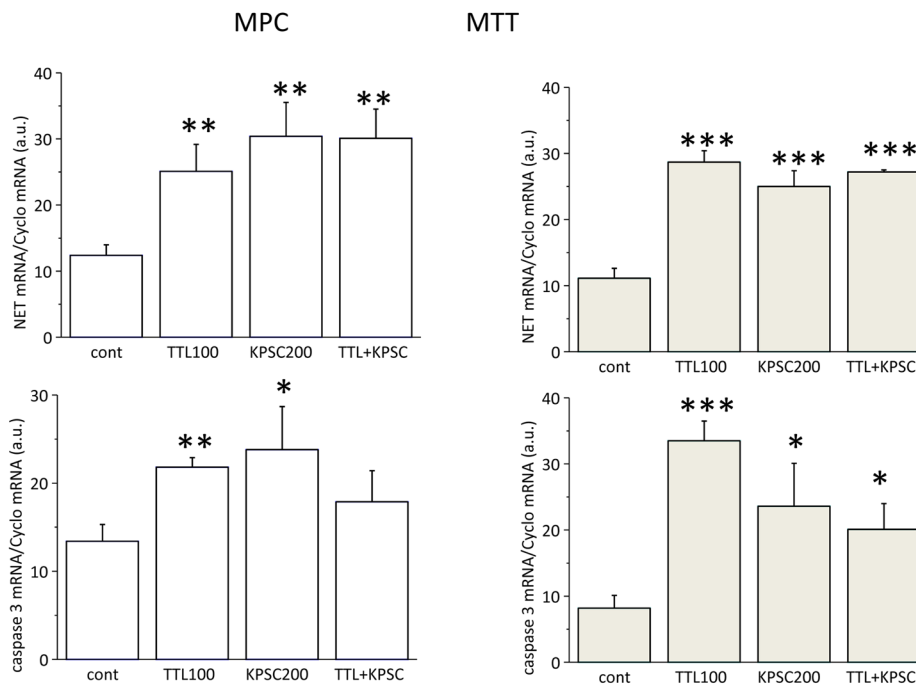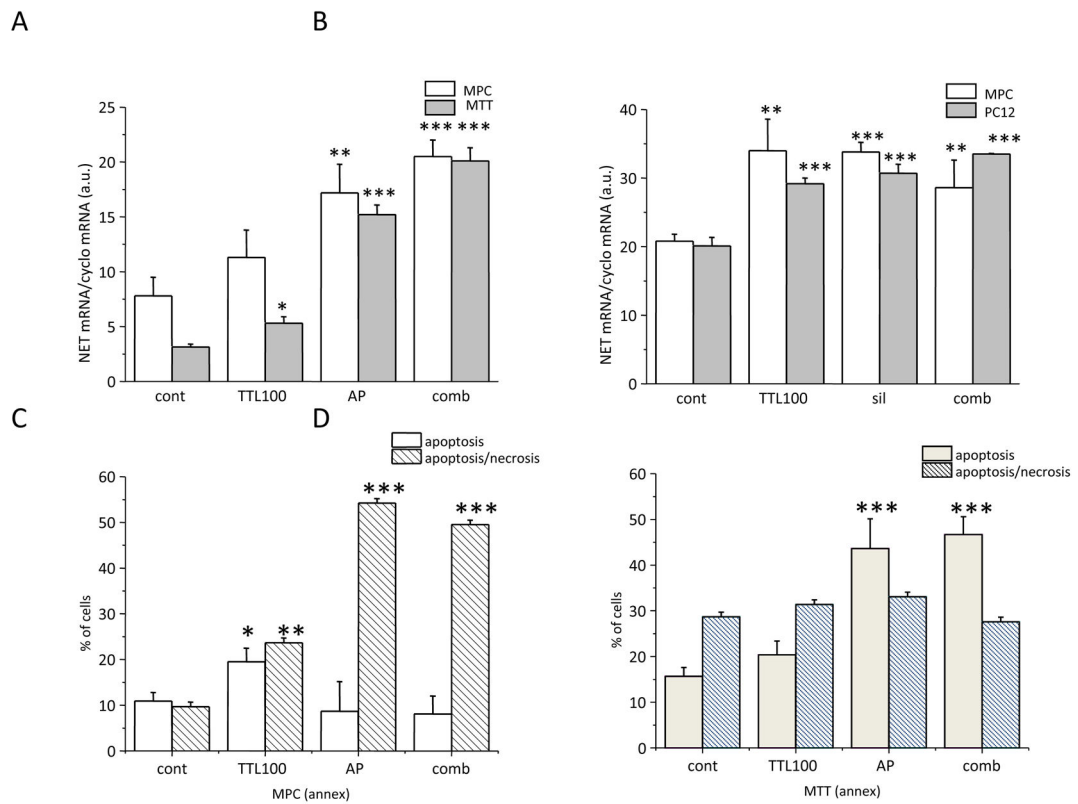
Figure 4.
Comparison of the effect of 100 nM TTL and 200 μM KPSC in MPC (**left**) and MTT (**right**) cells on NET mRNA (**upper part**) and caspase 3 mRNA (**bottom part**). In accordance with the TTL effect, KPSC also significantly increased both NET and caspase 3 mRNA. Results are displayed as mean ± S.E.M. and represent an average of at least five parallels from two independent cultivations. Statistical significance compared to control represents * - p>0.05, ** - p>0.01 and *** - p>0.001.

Figure 5.

Effect of NF-κB antisense peptide (AP; **A**) and NF-κB mRNA silencing (sil; **B**) on NET mRNA. In accordance with the TTL effect, AP and/or sil also significantly increased NET mRNA (**A, B**). In order to show that TTL acts through the NF-κB site, NET mRNA was measured in cells treated with a combination of both TTL and AP or sil (comb). In this combination, no additional increase in NET mRNA was observed as compared to TTL or AP or sil (**A, B**). Thus, based on this result we propose that TTL might act through the inhibition of the NF-κB site. In order to estimate the effect of AP on apoptosis and necrosis, we measured annexin V and propidium iodide in all tested samples (**C, D**). While AP significantly increased apoptosis in MTT cells (**D**), in MPC cells the same amount of AP resulted in an increase in necrosis (**C**). Results are displayed as mean ± S.E.M. and represent an average of at least five parallels from two independent cultivations. Statistical significance compared to control represents * - p>0.05, ** - p>0.01 and *** - p>0.001.
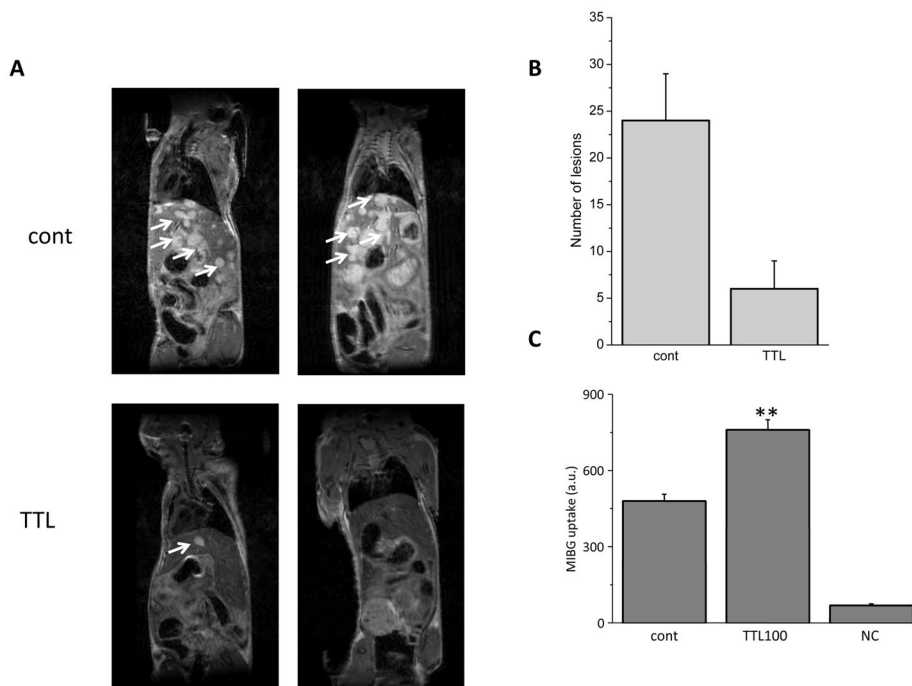
Figure 6.
In vivo efficacy study of TTL in an animal model of PHEO. Ten week old female nude mice were analyzed for liver metastases formation 5 weeks after tail vein injection of 5×10^5 MTT cells. **A)** Representative MRI images of two controls (upper images) and two TTL-treated (lower images) mice are shown. White arrows indicate the anatomical locations of some of the lesions inside the hepatic parenchyma. **B)** MRI images were analyzed using the OsiriX Imaging Software. The number of lesions in the livers was counted and plotted in a bar graph as mean ± S.E.M. **C)** MIBG uptake into control and TTL-treated MTT cells measured as the absorbance at 254 nm. TTL absorbance served as a negative control (NC). Results are displayed as mean ± S.E.M. and represent an average of at least five parallels from two independent cultivations. Statistical significance compared to control represents ** - p>0.01.
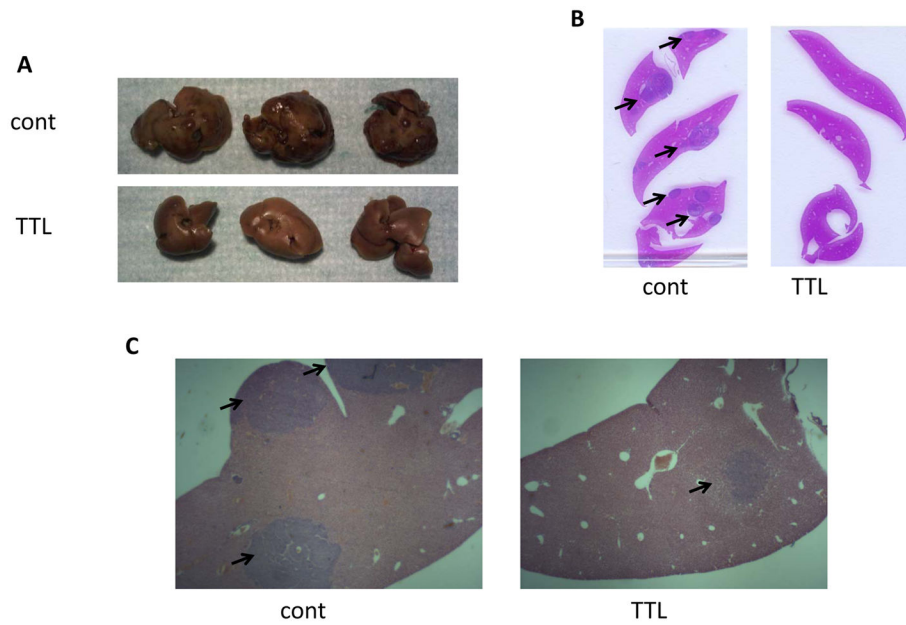
Figure 7.
Histopathological analysis of metastatic liver lesions in the PHEO mouse model. **A)** Gross anatomic images of the resected livers from untreated (control) and TTL-treated mice. The number of lesions visible on the hepatic surface of the control mice clearly contrasts with the absence of macroscopic lesions in the livers of treated mice. **B)** Livers were formalin fixed, embedded in paraffin and H&E stained; slices here represent control and TTL-treated animals. **C)** Representative images of histopathological sections (10x magnification) confirmed the higher presence of lesions in the control group as compared with the treated group. Black arrows indicate the anatomical location of the metastatic lesions in the liver.